HHS Public Access

Author manuscript

Neuropathol Appl Neurobiol. Author manuscript; available in PMC 2019 August 01.

Published in final edited form as:

Neuropathol Appl Neurobiol. 2018 August ; 44(5): 491–505. doi:10.1111/nan.12427.

Connexin-43 and Aquaporin-4 are markers of ARTAG-related astroglial response

Gabor G. Kovacs, MD PhD[1,2,¶], **Ahmed Yousef, BA**[2,¶], **Sabine Kaindl, BSc**[1], **Virginia M. Lee, PhD**[2], and **John Q. Trojanowski, MD PhD**[2,*]

[1]Institute of Neurology, Medical University of Vienna, Vienna, Austria

[2]Center for Neurodegenerative Disease Research, Institute on Aging and Department of Pathology and Laboratory Medicine of the Perelman School of Medicine at the University of Pennsylvania; Philadelphia, PA, USA

Abstract

Aims—Ageing-related tau astrogliopathy (ARTAG) appears in subependymal, subpial, perivascular, white matter (WM) and grey matter (GM) locations. Physical effects, blood-brain barrier dysfunction, blood- or vessel-related factors have been considered as aetiology. Since Connexin-43 (Cx43) and Aquaporin-4 (AQP4) are related to these, we hypothesized that their immunoreactivity varies with ARTAG in a location-specific manner.

Methods—We performed a morphometric immunohistochemical study measuring the densities of immunoreactivity (IR) of Cx43, AQP4, AT8 (phospho-tau), and glial fibrillar acidic protein (GFAP). We analysed the amygdala and hippocampus in age-matched cases with (n=19) and without (n=20) ARTAG in each of the locations it aggregates.

Results—We show a dramatic increase (> 6–fold; $p<0.01$) of Cx43 density of IR in ARTAG cases correlating strongly with AT8 density of IR, irrespective of the presence of neuronal tau pathology or reactive gliosis measured by GFAP density of IR, in the GM. In contrast, AQP4

Address correspondence to: Gabor G. Kovacs MD PhD, Institute of Neurology, Medical University of Vienna, AKH 4J, Währinger Gürtel 18-20, 1097 Vienna, Austria; gabor.kovacs@meduniwien.ac.at and John Q. Trojanowski MD PhD, Department of Pathology and Laboratory Medicine, Center for Neurodegenerative Disease Research, Institute on Aging, University of Pennsylvania School of Medicine, HUP Maloney 3rd Floor, 36th and Spruce Streets, Philadelphia, PA 19104 - 4283, USA; trojanow@mail.med.upenn.edu. DR GABOR G KOVACS (Orcid ID : 0000-0003-3841-5511)

[¶]These authors contributed equally to this work.

Ethics statement

The longitudinal Ageing VITA study included individuals after written consent of either the patient or the family or legal representative of the patient. Tissue samples were selected from the Brain Bank of the Institute of Neurology, Medical University of Vienna. The Ethical Committee of the Medical University of Vienna gave approval for neuropathological studies (Nr: 396/2011). All experiments were conducted according to the principles expressed in the Declaration of Helsinki, and in accordance with relevant Austrian guidelines and regulations, including the right to object from participating in scientific research. The manuscript does not contain information or images that could lead to an identification of the individual or which could violate any personal rights.

Conflict of interest: The authors report no conflict of interest.

Author Contributions

Gabor G. Kovacs: study design, acquisition of the data and statistical analysis, interpretation of the data, drafting the manuscript.
Ahmed Yousef: study design, acquisition of the data, interpretation of the data, drafting and revising the manuscript for content.
Sabine Kaindl: acquisition of the data, revising the manuscript for content.
Virginia M. Lee: revising the manuscript for content, study design, supervision.
John Q. Trojanowski: revising the manuscript for content, study design, interpretation of data, study supervision.

density of IR was increased only in the WM and GM, and was associated with increased AT8 density of IR only in WM and perivascular areas.

Discussion—Our study reveals distinctive astroglial responses in each of the locations associated with ARTAG. Our observations support the concept that factors related to brain-fluid interfaces and water-ion imbalances most likely play a role in the generation of ARTAG. Since Cx43 is crucial for maintaining neuronal homeostasis, the ARTAG-dependent increase of Cx43 density of IR suggests that the development of ARTAG in the GM most likely indicates an early response to the degeneration of neurons.

Keywords

ARTAG; aquaporin-4; blood-brain barrier; connexin 43; GFAP; Tau

Introduction

Pathological accumulation of abnormally phosphorylated tau protein in astrocytes has been frequently noted in the brains of elderly individuals. Recently, a consensus study described this as ageing-related tau astrogliopathy (ARTAG) [1]. Two morphologies—thorn-shaped astrocytes (TSA) and granular/fuzzy (GFA) astrocytes—were described. Furthermore, depending on the location, five types were defined: subependymal, subpial, perivascular, white matter (WM) and grey matter (GM) [1]. The aetiology of ARTAG has yet to be identified. However, physical effects (trauma), blood-brain barrier dysfunction, blood- or vessel-related factors have been suggested to affect its aggregations [2, 3]. Importantly, basal brain areas and particularly the amygdala are a hotspot for ARTAG [3].

Astrocytes play complex roles in the normal physiology of the brain as well as in reaction to pathologic events. Recent studies suggest a previously underestimated spectrum of functions and dysfunctions for astrocytes [4, 5]. These include a role in adaptive and regenerative CNS plasticity, synaptogenesis, neuronal migration, synaptic plasticity, support of the blood-brain barrier, secretion of trophic factors, regulation of local blood flow, ion exchange, and regulation of neurotransmitter homeostasis and glutamate levels [4, 5]. As a response to injury, astrogliosis contributes to neuroprotection and reconstruction of the compromised blood–brain barrier [4].

The most widely used immunohistochemical marker for the detection of astrocytes is glial fibrillar acidic protein (GFAP) [6]. However, there are further astrocytic markers, including connexin-43 (Cx43) and aquaporin-4 (AQP4). Cx43 is a protein highly expressed by astrocytes, especially at the interface of the blood-brain barrier [7]. It forms gap junctions and hemichannels, and it maintains the normal shape and function of astrocytes [8]. Importantly, connexin hemichannels are recognized as functional entities capable of influencing metabolic gradients within the nervous system, and they may play a role in the pathogenesis of neurodegenerative conditions [7, 8]. AQP4 is the member of water-channel proteins expressed in the foot processes of glial cells surrounding capillaries, and it is associated with water transfer into and out of the brain parenchyma [9]. Moreover, AQP4 is the target of pathogenic autoantibodies in the neuroinflammatory demyelinating disease neuromyelitis optica [10]. Based on these observations, we hypothesized that Cx43 and

AQP4 immunoreactivity varies with ARTAG in a location-dependent manner. To evaluate this, we performed a morphometric immunohistochemical study focusing on the amygdala and hippocampus and compared cases with and without different types of ARTAG.

Materials and Methods

Case selection

For this study 39 cases from the ongoing longitudinal VITA (Vienna Transdanubian Aging) study [11], which included individuals after written consent of either the patient or the family or legal representative of the patient, were selected from the Brain Bank of the Institute of Neurology, Medical University of Vienna. The Ethical Committee of the Medical University of Vienna gave approval for neuropathological studies (Nr: 396/2011). All experiments were conducted according to the principles expressed in the Declaration of Helsinki, and in accordance with relevant Austrian guidelines and regulations, including the right to object from participating in scientific research. The manuscript does not contain information or images that could lead to an identification of the individual or which could violate any personal rights. Neuropathological data for these cases are summarized in Table 1. We examined the hippocampus and amygdala. Nineteen cases showed varying ARTAG pathology. Twenty age-matched controls did not show ARTAG in any of the cortical, subcortical or brainstem areas, including the hippocampus and amygdala. Since not all cases develop all types of ARTAG pathology, not all ARTAG types were analysed in each case (Table 2). In addition, we performed immunostaining for Cx43 in three cases each with ischemic/hypoxic encephalopathy and Creutzfeldt-Jakob disease (Online supplemental file).

Immunohistochemistry

4-μm thick sections of formalin-fixed, paraffin-embedded tissue blocks containing either hippocampal regions or the amygdala and basal forebrain were cut and mounted on pre-coated glass slides (Star Frost, Waldemar Knittel GmbH, Braunschweig, Germany). We performed immunostaining for anti-phospho-tau (AT8; mouse monoclonal antibody (MAb); specific for pS202/pT205, 1:200, no pretreatment, Pierce Biotechnology, Rockford, IL, USA), anti-Cx43 (mouse MAb; 1:50, pretreatment pH 6.0 citrate buffer 10 min steamer, Invitrogen, Camarillo, CA, USA), anti-AQP4 (polyclonal rabbit antibody; 1:250, no pretreatment, Sigma-Aldrich, St. Louis, MO, USA), and GFAP (rabbit polyclonal; 1:3,000, pretreatment with Protease 5 min, Dako, Glostrup, Denmark). The antibody reactions were visualized either by DAKO EnVision© (K5007; for Cx4 and AQP4), or EnVision FLEX+© (K8002; for AT8 and GFAP) detection kit. Finally, sections were counterstained with haematoxylin.

Digital Image Acquisition

Digital images of histology slides were obtained using the bright-field function of a Lamina Multilabel slide scanner (Perkin Elmer; Waltham, MA) with a 20× objective. The images had a pixel resolution of 0.122 μm/pixel, camera resolution of 2560 × 2160, and a bit depth of 16. To create a smooth composite image, the composite image of each slide was autocorrected during the scan through the capture of 10 empty fields of view.

Semi-Automated Area Detection Algorithms and Selection of Regions of Analysis

Scanned slides were analysed using Halo digital image software v2.0.1061.3 (Indica Labs; Albuquerque, NM). Halo was utilized to develop detection algorithms to quantify immunoreactivity of AT8, Cx43, and AQP4 using the "Area Quantification" v1.0 setting. Previous work has validated the utility of this tool in the detection of pathology in human paraffin-embedded tissue [12]. For each antibody, stains of interest were programed in the algorithm based on red, green, and blue optical density for colour deconvolution to isolate chromogen signals from their counterstain. Thresholds for positive optical density were determined by visual inspection and cross-validated by two investigators (GGK, AY). Although Halo allows for three threshold levels for optical density (i.e., yellow as weak, orange as moderate, red as strong), all positive signals were set as strong. The algorithms were adjusted to ensure minimal detection of negative background. Positive signal was measured as the percentage area occupied and was reported as density of immunoreactivity (IR). Representative images of the algorithms' detection of immunoreactivity are shown in Fig 1. For each tissue analysed, the regions of interest included the perivascular, subependymal, subpial, grey matter, and white matter regions. The different ARTAG types were annotated for analysis using Halo's "pen" tool. Representative samples of each ARTAG type were sampled in each case. To allow for comparisons between each examined antibody's reactivity in the same region of interest, corresponding selections were made in sequential tissue using Halo's "synchronize navigation" tool. For perivascular regions, the size of the selected region was appropriately adjusted due to variation between sequential sections.

Statistical analysis

Mann-Whitney (M-W) tests were used to compare ARTAG to controls. Linear logistic regression tests were performed to evaluate the effect of examined variables on the expression of Cx43 and AQP4. Spearman tests were performed to evaluate the correlation and association between variables. The software SPSS Statistics (V23.0, SPSS Inc., Chicago, IL, USA) was used for these analyses. Significance was set to $p=0.05$.

Results

In total, 238 images (117 from cases with ARTAG) were analysed. The anatomical distribution of locations (representing ARTAG types) examined is summarized in Table 2.

Immunostaining for AT8 and GFAP

In the ARTAG group, immunostaining for AT8 revealed astrocytic tau immunoreactivity in subependymal, subpial, perivascular, WM and GM locations. Variable amounts of neuropil threads, fine granular cytoplasmic or neurofibrillary tangle-like neuronal tau pathology in the GM, and fine thread-like profiles in the WM were observed in both ARTAG and control groups. In addition, in the control group, occasional scattered fine dots were seen in subependymal and subpial locations. Comparison of all AT8 images of ARTAG cases to controls showed significantly higher tau load in ARTAG pooled cases (Fig. 2A; M-W: $p<0.0011$) and in all examined locations (Fig. 2B; M-W: $p<0.01$ for all). Importantly, GM areas did not show dystrophic neurites or amyloid plaques. Immunostaining for GFAP

showed astrocytes, including a few with hypertrophic morphology correlating with mild to moderate neuronal loss in the amygdala. GFAP DIR was significantly higher in ARTAG pooled cases (Fig. 2A; M-W: $p<0.01$). When comparing different locations, except for subependymal, all showed higher GFAP DIR values in ARTAG (Fig. 2C; M-W: $p<0.01$ for perivascular and GM and $p<0.05$ for subpial and WM).

Distinct immunostaining for Cx43 in ARTAG cases

Immunostaining for Cx43 revealed fine dots in astrocytic processes. When all images were pooled, Cx43 DIR was increased more than 6-fold in ARTAG (Fig. 2A; M-W: $p<0.0011$). When compared to GFAP, the DIR of Cx43 was much less (around 20-fold). When comparing different locations, with the exception of subependymal (M-W: $p=0.35$), all other locations showed higher Cx43 DIR in ARTAG cases (Fig. 2D; M-W: $p<0.01$ for perivascular, WM, and GM and $p<0.05$ for subpial; Figs. 3–5). When all examined locations were pooled, a Spearman test revealed significant ($p<0.05$) correlations between Cx43, GFAP and AQP4 DIR in both ARTAG and control cases, as well as with AT8 DIR in ARTAG cases (Table 3). Spearman tests also revealed strong correlations between Cx43 DIR with the DIR of GFAP, AT8, and AQP4 in ARTAG cases in subpial, perivascular, WM and GM locations. In controls, Cx43 DIR correlated only with GFAP DIR (Table 3). Additionally, we analysed each ARTAG type using a linear logistic regression model for Cx43 DIR where AT8 and GFAP DIR were included as multiple variables. For subependymal ARTAG, none showed an effect ($p>0.6$ for both). For subpial ARTAG, only GFAP DIR showed a significant effect ($p=0.014$). For perivascular, WM and GM ARTAG, only AT8 DIR showed a significant effect ($p<0.01$ for all) independent of GFAP DIR. Additional immunostainings for Cx43 in cases with prominent reactive astrogliosis due to ischemic/hypoxic encephalopathy and Creutzfeldt-Jakob disease did not reveal corresponding enhancement of Cx43 immunoreactivity (Online supplemental file). In addition, the effect of AT8 on Cx43 DIR in the GM was independent of the presence (yes/no) of neuronal tau pathology (included in the model as an additional variable). Finally, in linear logistic regression models, including those with multiple variables such as AT8 DIR, we did not observe any effect of the presence of argyrophilic grains, TDP-43 pathology, or dementia ($p>0.1$ for all) on Cx43 DIR while adding subregion analysis to the model did not change the results.

Distinct immunostaining for AQP4 in ARTAG cases

Immunostaining for AQP4 revealed astrocytic cytoplasms and processes in both controls and ARTAG cases. When all images were pooled, AQP4 DIR was moderately (1.36-fold) but significantly increased in the ARTAG group (Figure 2A; M-W: $p<0.01$). GFAP DIR was around 1.5–1.8-fold higher than AQP4 DIR. When comparing different locations, AQP4 DIR was higher in WM and GM locations in ARTAG cases (Figure 2E; M-W: $p<0.05$; Figures 3–5), but not in other locations (M-W: $p=0.60$, 0.73, and 0.15 for subependymal, subpial, and perivascular, respectively). When all examined locations were pooled, Spearman tests revealed significant ($p<0.05$) correlations between AQP4, GFAP, AT8 and Cx43 DIR in both ARTAG and control cases (Table 3). When the locations were evaluated separately, with the exception of the subependymal location, AQP4 DIR strongly correlated with Cx43 DIR. Also, with the exception of the GM and subependymal locations, AQP4

DIR correlated with GFAP DIR in ARTAG cases (Table 3). Except for in the WM, AQP4 did not correlate with AT8 DIR in ARTAG cases. We also evaluated ARTAG types using a linear logistic regression model for AQP4 DIR with AT8 and GFAP DIR as multiple variables. For subependymal ARTAG, none showed an effect ($p>0.6$ for both); for subpial ARTAG, only GFAP DIR showed a significant effect ($p=0.001$); and for perivascular and WM ($p<0.05$ for both) but not GM ($p= 0.093$), ARTAG AT8 DIR showed significant effects independent of GFAP DIR. As for Cx43, further pathological variables did not show any effect ($p>0.1$ for all) on AQP4 DIR.

Discussion

The concept of ARTAG was introduced to facilitate research on the understanding of the role of astrocytes in neurodegeneration and brain ageing [1]. In particular, ARTAG may be seen in aged brains without other proteinopathies or Alzheimer disease (AD). Peculiar forms of widespread or circumscribed GM ARTAG seem to be associated with dementia or focal symptoms [13, 14]. ARTAG is not unique to humans. Tau-positive astrocytes, strongly reminiscent of ARTAG, have been described in perivascular, subpial, and subependymal locations in aged baboons [15]. Moreover, the presence of glial tau pathology co-occurring with amyloid plaques in aged gorillas suggests that age-related tau changes in gorillas evolves independently from amyloid-related plaque pathology [16].

ARTAG in different locations in the ageing brain most likely reflects different pathogenic events. Frequent ARTAG pathology in subpial and perivascular locations particularly in basal areas may be suggestive of blood-brain barrier dysfunction, water transport, or blood- or vessel-related factors [3]. Likewise, subpial ARTAG, particularly in lobar areas, shows considerable overlap with tau pathologies described in chronic traumatic encephalopathy (CTE) [2, 3, 17]. Moreover, GM ARTAG can be a link to a better understanding of astrocytic tau pathologies in primary frontotemporal lobar degeneration tauopathies such as progressive supranuclear palsy or corticobasal degeneration [3]. To gain insights into the pathogenesis of ARTAG, in the present study, we evaluated two astroglial markers and found distinctive changes. Since there is still variability in evaluating astrocytic tau pathologies [18], the major aim was to define a marker for ARTAG, in particular in WM and GM location. On the one hand, we sought to understand pathogenesis, and on the other hand to provide a basis for comparison with disease states, including primary FTLD-tauopathies, to better understand the overlap of astrocytic tau morphologies with ARTAG [3].

Cx43 and AQP4 have been examined in brain disorders, such as epilepsy, neuroinflammatory conditions, and brain oedema [9, 19]. Less data are available for neurodegenerative conditions in the human brain. Nagy et al. reported that Cx43 immunostaining patterns in AD brains are mainly associated with amyloid plaques [20]. Another study reported increased Cx43 expression appearing as patches in the caudate nucleus contrasting the globus pallidus in Huntington`s disease [21]. Increased AQP4 expression has been recently reported as a feature of the ageing human brain, and its mislocalization was related to the development of AD plaque-pathology [22]. Other studies have reported that AQP4 is not only important for the clearance of Amyloid-β in the brain via lymphatic pathways but is essential for synaptic function as well [23].

Connexins are constituents of gap junctions [19]. Different isoforms are distinguished, with Cx43 being a major form associated with astrocytes that have been linked to several processes that impact both brain homeostasis and repair after injury [19]. Cx43 is considered an immunregulating factor at the gliovascular, i.e., blood-brain barrier, interface [24] and contributes to the release of gliotransmitters [25]. We show that Cx43 DIR is increased in ARTAG cases when compared to controls in the subpial, perivascular, WM, and GM locations. Importantly, for perivascular, WM and GM ARTAG, correlation of Cx43 and AT8 DIR is independent from GFAP DIR. This is further supported by the lack of enhanced Cx43 immunoreactivity of reactive astrocytes in ischemic/hypoxic encephalopathy and Creutzfeldt-Jakob diseased brains (see Online supplemental file). Therefore, this is not a mere increase related to reactive changes of astrocytes. Furthermore, there was a lack of significant Cx43 DIR difference in the subependymal location. This likely reflects an age-related increase of Cx43 expression associated with a life-long preparedness of subependymal astrocytes for events affecting the ependymal [26, 27], where the development of ARTAG does not further increase Cx43 expression. It can be hypothesized that the elevated Cx43 DIR in perivascular, WM and GM locations reflects a response to blood-brain barrier dysfunction or to local hypoperfusion. However, particularly relevant for the interpretation of GM ARTAG, observations in experimental models of AD suggest that Cx43 expression may promote neuronal survival, for example, by sensing and reducing elevated levels of extracellular glutamate [28]. In stroke models, Cx43 can stabilize astrocytes and facilitate the resistance to the deleterious effects of a stroke-like milieu and promote neuronal recovery [29]. Therefore, the appearance of hyperphosphorylated tau pathology in the form of GM ARTAG, together with increased Cx43 expression, might be indicative of a neuroprotective mechanism of astrocytes to minimize the toxicity of the extracellular space through spatial buffering [19]. Interestingly, in our recent comprehensive study on ARTAG, we observed GM ARTAG in anatomical regions without neuronal tau pathology [3], as reported also in corticobasal degeneration [30]. Indeed, here we show that increased Cx43 expression is associated with GM ARTAG irrespective of the presence of neuronal tau pathology. On the other hand, the progressive increase in Cx43 expression in the SOD1 (G93A) mouse model of amyotrophic lateral sclerosis (ALS) and in the motor cortex and spinal cord of ALS patients during the disease course was interpreted as astrocyte-mediated toxicity [31]. Since astroglial gap junctions seem to provide an activity-dependent intercellular pathway for the delivery of energetic metabolites from blood vessels to distal neurons [32], the ARTAG-related increase of Cx43 DIR might also be an early response to neuronal degeneration.

In contrast to Cx43, AQP4 DIR was significantly higher only in WM and GM locations in ARTAG cases. AQP4 is a channel protein primarily associated with brain-fluid (blood or cerebrospinal fluid) interfaces and water transport into and out of the brain parenchyma; thus, it interfaces with astrocytes predominantly at the perivascular end-feet in direct contact with blood vessels [9, 33, 34]. Therefore, strong AQP4 expression in subependymal, subpial and perivascular locations is physiological, and we were unable to demonstrate a significant increase in AQP4 DIR in ARTAG cases. In the WM and perivascular locations, however, the presence of AT8-positive astrocytes was associated with increased AQP4 DIR. This supports the notion that in the WM and perivascular locations, ARTAG might be related to pathogenic

events associated with the blood-brain barrier (i.e. dysfunction or inflow of yet unidentified factors). In the GM, the increase of AQP4 in ARTAG cases could be suggestive of blood-brain barrier dysfunction. However, additional pathogeneses should be also considered, since AQP4 alone, is not a sufficient correlate for increased amount of GM ARTAG (i.e., lack of correlation with AT8 DIR). Limitations of our study include challenging aspects of quantitative immunohistochemistry, since, for example, antigens like AQP4 can show background staining or immunoreactivity might vary with prolonged formalin fixation times. To avoid these pitfalls we included cases from a longitudinal ageing study, where sampling and processing were standardized.

In summary, our study reveals distinctive astroglial responses in different locations associated with ARTAG. Our observations support the concept that factors related to the brain-fluid interfaces including blood-brain barrier and water-ion imbalances most likely play a role in the generation of ARTAG, not only in subependymal and subpial but also in WM and perivascular locations. Importantly, we evaluated age-matched cases from a community-based study and not all cases developed ARTAG in subependymal or subpial locations suggesting that a yet unidentified factor (i.e. not a pure ageing effect) is needed for this. In this study, we evaluated basal areas of the brain (amygdala and hippocampus); the pathogenesis of subpial ARTAG in dorsolateral areas of lobes (e.g., frontal) might involve further pathogenic components (e.g., microtrauma) [1, 3]. Indeed, the development of ARTAG in the GM likely involves further changes and might reflect an early response to degeneration of neurons. We expand the observations of Cx43- and AQP4-related astrocytic responses in human neurodegenerative conditions [9, 20–22, 31] and suggest that GM ARTAG is a preceding marker of neuronal degeneration [3]. The clarification of whether this is an early neuroprotective response of astrocytes or if this is a factor contributing to neurotoxicity merits further studies.

Supplementary Material

Refer to Web version on PubMed Central for supplementary material.

Acknowledgments

Support for this work was provided by grants from the National Institute on Aging of the National Institutes of Health (P30-AG10124, PO1-AG17586, NS088341 and NS094003).

References

1. Kovacs GG, Ferrer I, Grinberg LT, Alafuzoff I, Attems J, Budka H, Cairns NJ, Crary JF, Duyckaerts C, Ghetti B, Halliday GM, Ironside JW, Love S, Mackenzie IR, Munoz DG, Murray ME, Nelson PT, Takahashi H, Trojanowski JQ, Ansorge O, Arzberger T, Baborie A, Beach TG, Bieniek KF, Bigio EH, Bodi I, Dugger BN, Feany M, Gelpi E, Gentleman SM, Giaccone G, Hatanpaa KJ, Heale R, Hof PR, Hofer M, Hortobagyi T, Jellinger K, Jicha GA, Ince P, Kofler J, Kovari E, Kril JJ, Mann DM, Matej R, McKee AC, McLean C, Milenkovic I, Montine TJ, Murayama S, Lee EB, Rahimi J, Rodriguez RD, Rozemuller A, Schneider JA, Schultz C, Seeley W, Seilhean D, Smith C, Tagliavini F, Takao M, Thal DR, Toledo JB, Tolnay M, Troncoso JC, Vinters HV, Weis S, Wharton SB, White CL 3rd, Wisniewski T, Woulfe JM, Yamada M, Dickson DW. Aging-related tau astrogliopathy (ARTAG): harmonized evaluation strategy. Acta Neuropathol. 2016; 131:87–102. [PubMed: 26659578]

2. Liu AK, Goldfinger MH, Questari HE, Pearce RK, Gentleman SM. ARTAG in the basal forebrain: widening the constellation of astrocytic tau pathology. Acta Neuropathol Commun. 2016; 4:59. [PubMed: 27297017]

3. Kovacs GG, Robinson JL, Xie SX, Lee EB, Grossman M, Wolk DA, Irwin DJ, Weintraub D, Kim CF, Schuck T, Yousef A, Wagner ST, Suh E, Van Deerlin VM, Lee VM, Trojanowski JQ. Evaluating the Patterns of Aging-Related Tau Astrogliopathy Unravels Novel Insights Into Brain Aging and Neurodegenerative Diseases. J Neuropathol Exp Neurol. 2017; doi: 10.1093/jnen/nlx007

4. Pekny M, Pekna M, Messing A, Steinhauser C, Lee JM, Parpura V, Hol EM, Sofroniew MV, Verkhratsky A. Astrocytes: a central element in neurological diseases. Acta Neuropathol. 2016; 131:323–45. [PubMed: 26671410]

5. Sofroniew MV, Vinters HV. Astrocytes: biology and pathology. Acta Neuropathol. 2010; 119:7–35. [PubMed: 20012068]

6. Ben Haim L, Carrillo-de Sauvage MA, Ceyzeriat K, Escartin C. Elusive roles for reactive astrocytes in neurodegenerative diseases. Front Cell Neurosci. 2015; 9:278. [PubMed: 26283915]

7. Orellana JA, Retamal MA, Moraga-Amaro R, Stehberg J. Role of Astroglial Hemichannels and Pannexons in Memory and Neurodegenerative Diseases. Front Integr Neurosci. 2016; 10:26. [PubMed: 27489539]

8. Takeuchi H, Suzumura A. Gap junctions and hemichannels composed of connexins: potential therapeutic targets for neurodegenerative diseases. Front Cell Neurosci. 2014; 8:189. [PubMed: 25228858]

9. Tang G, Yang GY. Aquaporin-4: A Potential Therapeutic Target for Cerebral Edema. Int J Mol Sci. 2016; 17

10. Tradtrantip L, Jin BJ, Yao X, Anderson MO, Verkman AS. Aquaporin-Targeted Therapeutics: State-of-the-Field. Adv Exp Med Biol. 2017; 969:239–50. [PubMed: 28258578]

11. Kovacs GG, Milenkovic I, Wohrer A, Hoftberger R, Gelpi E, Haberler C, Honigschnabl S, Reiner-Concin A, Heinzl H, Jungwirth S, Krampla W, Fischer P, Budka H. Non-Alzheimer neurodegenerative pathologies and their combinations are more frequent than commonly believed in the elderly brain: a community-based autopsy series. Acta Neuropathol. 2013; 126:365–84. [PubMed: 23900711]

12. Irwin DJ, Byrne MD, McMillan CT, Cooper F, Arnold SE, Lee EB, Van Deerlin VM, Xie SX, Lee VM, Grossman M, Trojanowski JQ. Semi-Automated Digital Image Analysis of Pick's Disease and TDP-43 Proteinopathy. J Histochem Cytochem. 2016; 64:54–66. [PubMed: 26538548]

13. Kovacs GG, Molnar K, Laszlo L, Strobel T, Botond G, Honigschnabl S, Reiner-Concin A, Palkovits M, Fischer P, Budka H. A peculiar constellation of tau pathology defines a subset of dementia in the elderly. Acta Neuropathol. 2011; 122:205–22. [PubMed: 21437732]

14. Munoz DG, Woulfe J, Kertesz A. Argyrophilic thorny astrocyte clusters in association with Alzheimer's disease pathology in possible primary progressive aphasia. Acta Neuropathol. 2007; 114:347–57. [PubMed: 17637999]

15. Schultz C, Hubbard GB, Tredici KD, Braak E, Braak H. Tau pathology in neurons and glial cells of aged baboons. Adv Exp Med Biol. 2001; 487:59–69. [PubMed: 11403166]

16. Perez SE, Raghanti MA, Hof PR, Kramer L, Ikonomovic MD, Lacor PN, Erwin JM, Sherwood CC, Mufson EJ. Alzheimer's disease pathology in the neocortex and hippocampus of the western lowland gorilla (Gorilla gorilla gorilla). J Comp Neurol. 2013; 521:4318–38. [PubMed: 23881733]

17. McKee AC, Cairns NJ, Dickson DW, Folkerth RD, Keene CD, Litvan I, Perl DP, Stein TD, Vonsattel JP, Stewart W, Tripodis Y, Crary JF, Bieniek KF, Dams-O'Connor K, Alvarez VE, Gordon WA. group TC. The first NINDS/NIBIB consensus meeting to define neuropathological criteria for the diagnosis of chronic traumatic encephalopathy. Acta Neuropathol. 2016; 131:75–86. [PubMed: 26667418]

18. Kovacs GG, Xie SX, Lee EB, Robinson JL, Caswell C, Irwin DJ, Toledo JB, Johnson VE, Smith DH, Alafuzoff I, Attems J, Bencze J, Bieniek KF, Bigio EH, Bodi I, Budka H, Dickson DW, Dugger BN, Duyckaerts C, Ferrer I, Forrest SL, Gelpi E, Gentleman SM, Giaccone G, Grinberg LT, Halliday GM, Hatanpaa KJ, Hof PR, Hofer M, Hortobagyi T, Ironside JW, King A, Kofler J, Kovari E, Kril JJ, Love S, Mackenzie IR, Mao Q, Matej R, McLean C, Munoz DG, Murray ME, Neltner J, Nelson PT, Ritchie D, Rodriguez RD, Rohan Z, Rozemuller A, Sakai K, Schultz C,

Seilhean D, Smith V, Tacik P, Takahashi H, Takao M, Rudolf Thal D, Weis S, Wharton SB, White CL 3rd, Woulfe JM, Yamada M, Trojanowski JQ. Multisite Assessment of Aging-Related Tau Astrogliopathy (ARTAG). J Neuropathol Exp Neurol. 2017

19. Freitas-Andrade M, Naus CC. Astrocytes in neuroprotection and neurodegeneration: The role of connexin43 and pannexin1. Neuroscience. 2016; 323:207–21. [PubMed: 25913636]
20. Nagy JI, Li W, Hertzberg EL, Marotta CA. Elevated connexin43 immunoreactivity at sites of amyloid plaques in Alzheimer's disease. Brain Res. 1996; 717:173–8. [PubMed: 8738268]
21. Vis JC, Nicholson LF, Faull RL, Evans WH, Severs NJ, Green CR. Connexin expression in Huntington's diseased human brain. Cell Biol Int. 1998; 22:837–47. [PubMed: 10873295]
22. Zeppenfeld DM, Simon M, Haswell JD, D'Abreo D, Murchison C, Quinn JF, Grafe MR, Woltjer RL, Kaye J, Iliff JJ. Association of Perivascular Localization of Aquaporin-4 With Cognition and Alzheimer Disease in Aging Brains. JAMA Neurol. 2017; 74:91–9. [PubMed: 27893874]
23. Yang C, Huang X, Huang X, Mai H, Li J, Jiang T, Wang X, Lu T. Aquaporin-4 and Alzheimer's Disease. J Alzheimers Dis. 2016; 52:391–402. [PubMed: 27031475]
24. Boulay AC, Cisternino S, Cohen-Salmon M. Immunoregulation at the gliovascular unit in the healthy brain: A focus on Connexin 43. Brain Behav Immun. 2016; 56:1–9. [PubMed: 26674996]
25. Stehberg J, Moraga-Amaro R, Salazar C, Becerra A, Echeverria C, Orellana JA, Bultynck G, Ponsaerts R, Leybaert L, Simon F, Saez JC, Retamal MA. Release of gliotransmitters through astroglial connexin 43 hemichannels is necessary for fear memory consolidation in the basolateral amygdala. FASEB J. 2012; 26:3649–57. [PubMed: 22665389]
26. Miragall F, Albiez P, Bartels H, de Vries U, Dermietzel R. Expression of the gap junction protein connexin43 in the subependymal layer and the rostral migratory stream of the mouse: evidence for an inverse correlation between intensity of connexin43 expression and cell proliferation activity. Cell Tissue Res. 1997; 287:243–53. [PubMed: 8995195]
27. Roales-Bujan R, Paez P, Guerra M, Rodriguez S, Vio K, Ho-Plagaro A, Garcia-Bonilla M, Rodriguez-Perez LM, Dominguez-Pinos MD, Rodriguez EM, Perez-Figares JM, Jimenez AJ. Astrocytes acquire morphological and functional characteristics of ependymal cells following disruption of ependyma in hydrocephalus. Acta Neuropathol. 2012; 124:531–46. [PubMed: 22576081]
28. Peters O, Schipke CG, Philipps A, Haas B, Pannasch U, Wang LP, Benedetti B, Kingston AE, Kettenmann H. Astrocyte function is modified by Alzheimer's disease-like pathology in aged mice. J Alzheimers Dis. 2009; 18:177–89. [PubMed: 19584439]
29. Wu LY, Yu XL, Feng LY. Connexin 43 stabilizes astrocytes in a stroke-like milieu to facilitate neuronal recovery. Acta Pharmacol Sin. 2015; 36:928–38. [PubMed: 26095039]
30. Ling H, Kovacs GG, Vonsattel JP, Davey K, Mok KY, Hardy J, Morris HR, Warner TT, Holton JL, Revesz T. Astrogliopathy predominates the earliest stage of corticobasal degeneration pathology. Brain. 2016; 139:3237–52. [PubMed: 27797812]
31. Almad AA, Doreswamy A, Gross SK, Richard JP, Huo Y, Haughey N, Maragakis NJ. Connexin 43 in astrocytes contributes to motor neuron toxicity in amyotrophic lateral sclerosis. Glia. 2016; 64:1154–69. [PubMed: 27083773]
32. Rouach N, Koulakoff A, Abudara V, Willecke K, Giaume C. Astroglial metabolic networks sustain hippocampal synaptic transmission. Science. 2008; 322:1551–5. [PubMed: 19056987]
33. Verkman AS. Aquaporins at a glance. J Cell Sci. 2011; 124:2107–12. [PubMed: 21670197]
34. Verkman AS, Binder DK, Bloch O, Auguste K, Papadopoulos MC. Three distinct roles of aquaporin-4 in brain function revealed by knockout mice. Biochim Biophys Acta. 2006; 1758:1085–93. [PubMed: 16564496]

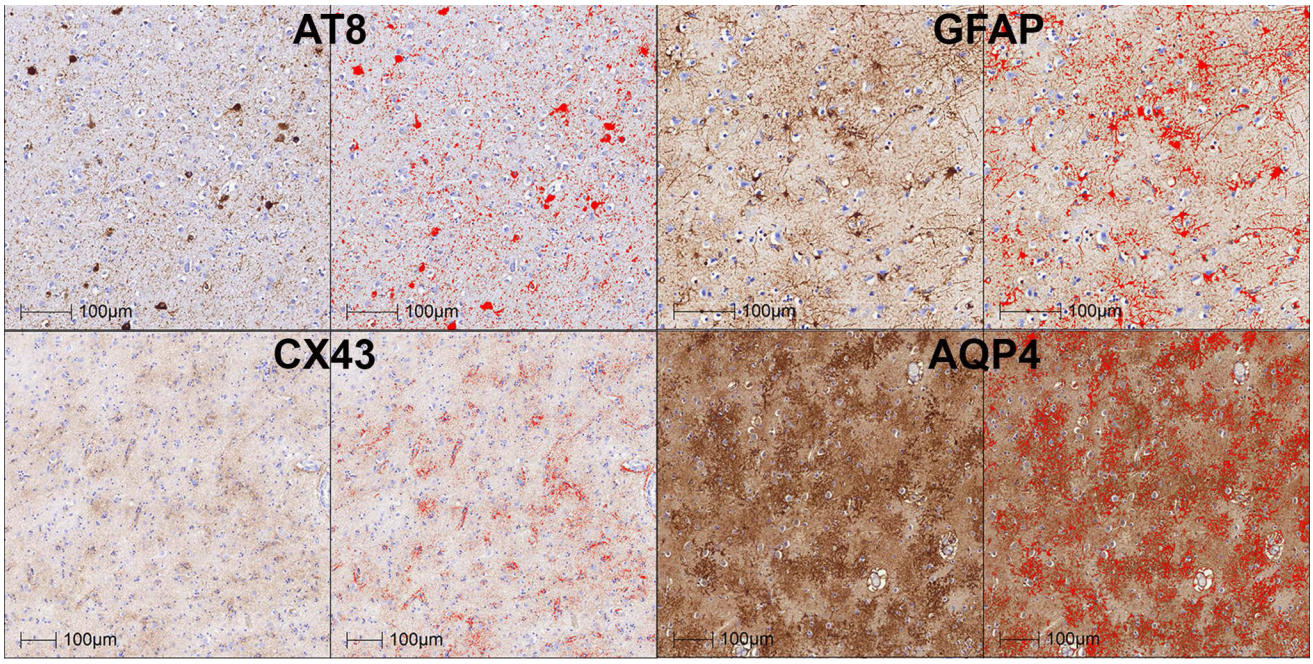

Fig 1.

Representative images (amygdala of CO-20 for AT8; hippocampus of ARTAG-17 for Cx43; hippocampus of ARTAG-3 for AQP4; hippocampus of CO-7 for GFAP; see Table 1) of the morphometric algorithms' detection of immunoreactivities. Red colour indicates the immunoreactivities, which were detected and used for density measurements.

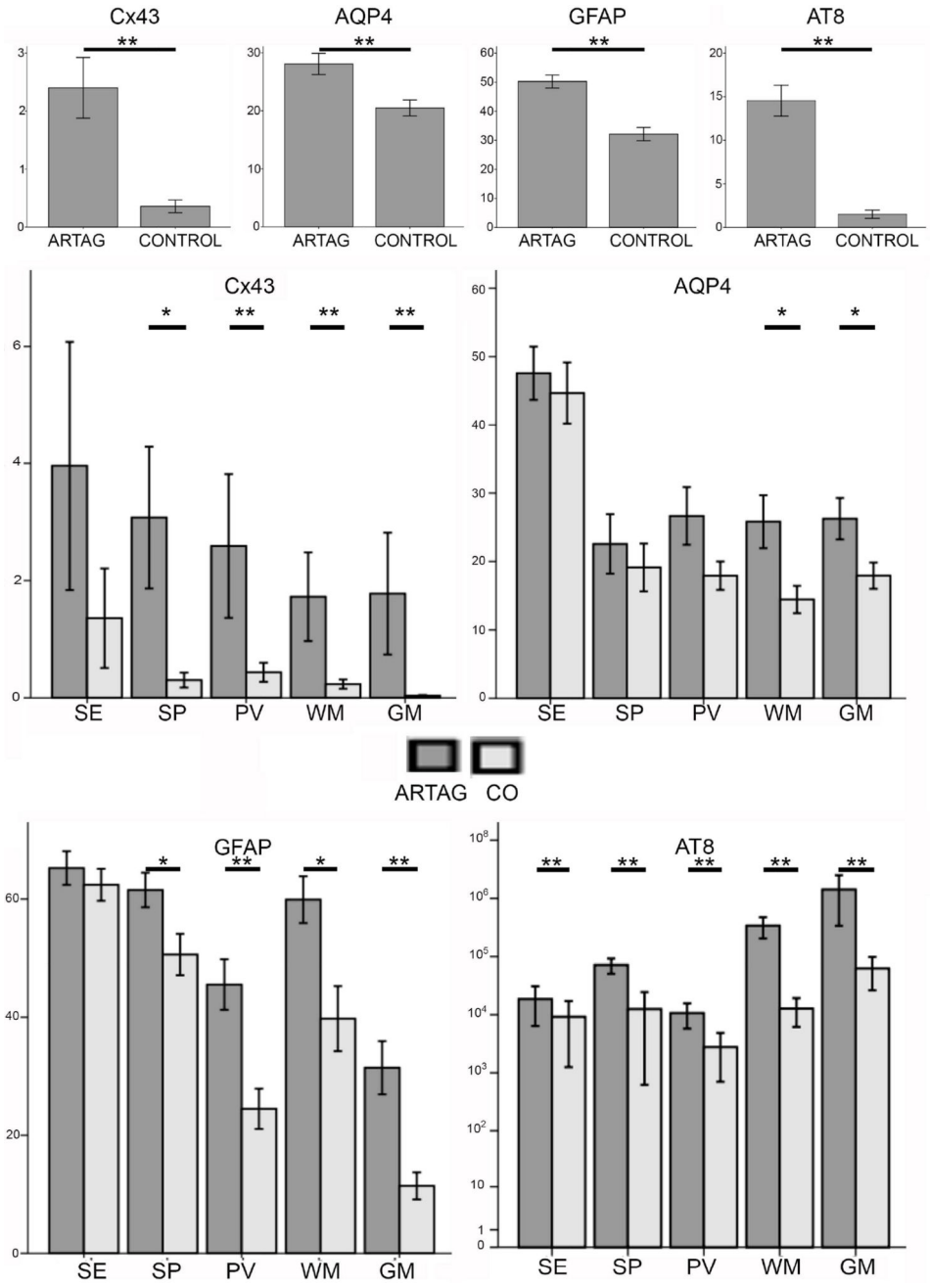

Fig 2.

Graphical representation of densities of immunoreactivities (DIR) of AT8, GFAP, Cx43 and AQP4 in ARTAG and controls in different locations (SE: subependymal; SP: subpial; PV: perivascular; WM: white matter; GM: grey matter). * indicates $p<0.05$ and ** $p< 0.01$.

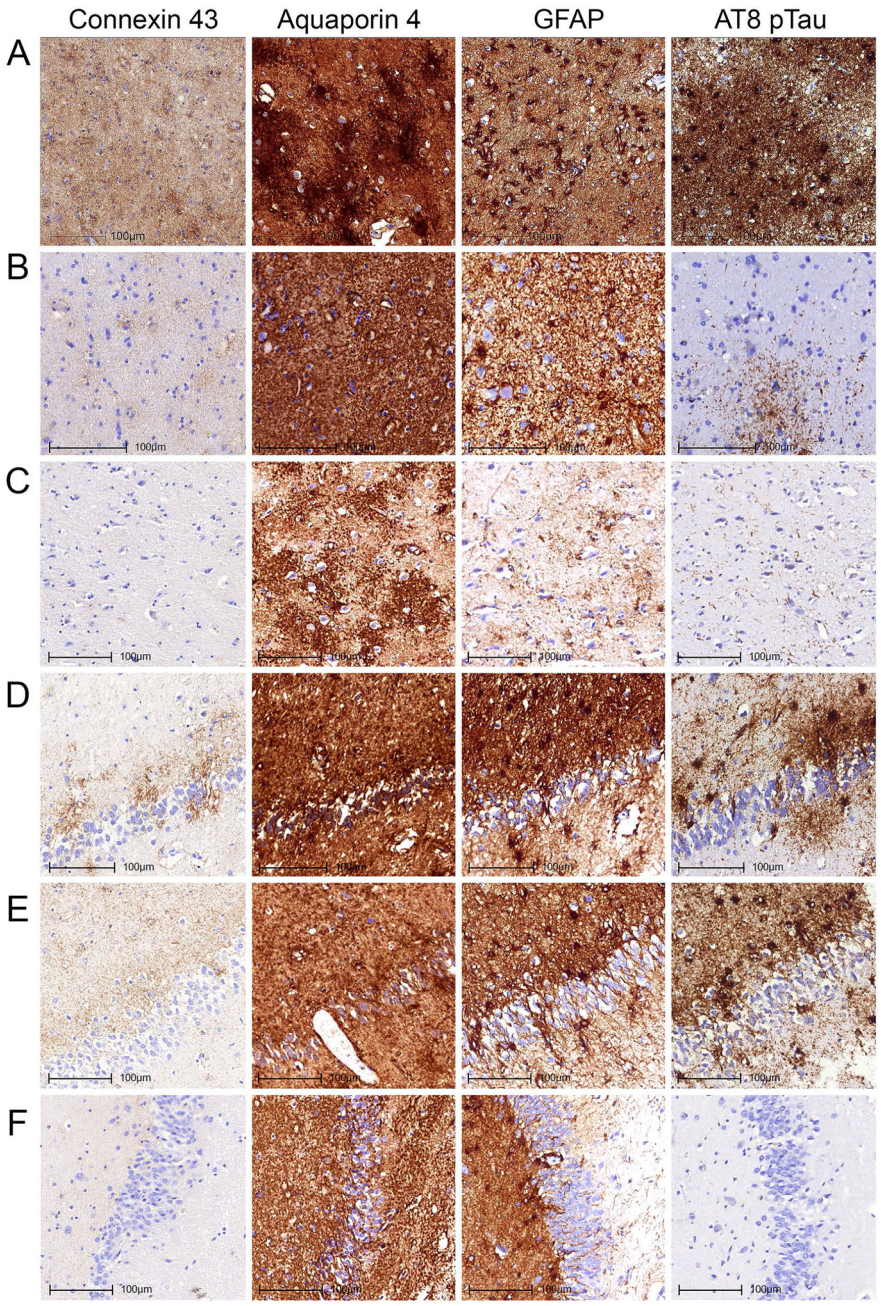

Fig 3.

Immunostaining patterns of Cx43, AQP4, GFAP and AT8 pTau in the amygdala (A–C) and dentate gyrus of the hippocampus (D–F) representing different degrees of burden of tau pathologies. Images A and D represent case ARTAG-2 demonstrating prominent grey matter ARTAG, B represents case ARTAG-16 and E represents case ARTAG-1 demonstrating moderate degree of grey matter ARTAG; C and F represents case CO-5 lacking grey matter ARTAG.

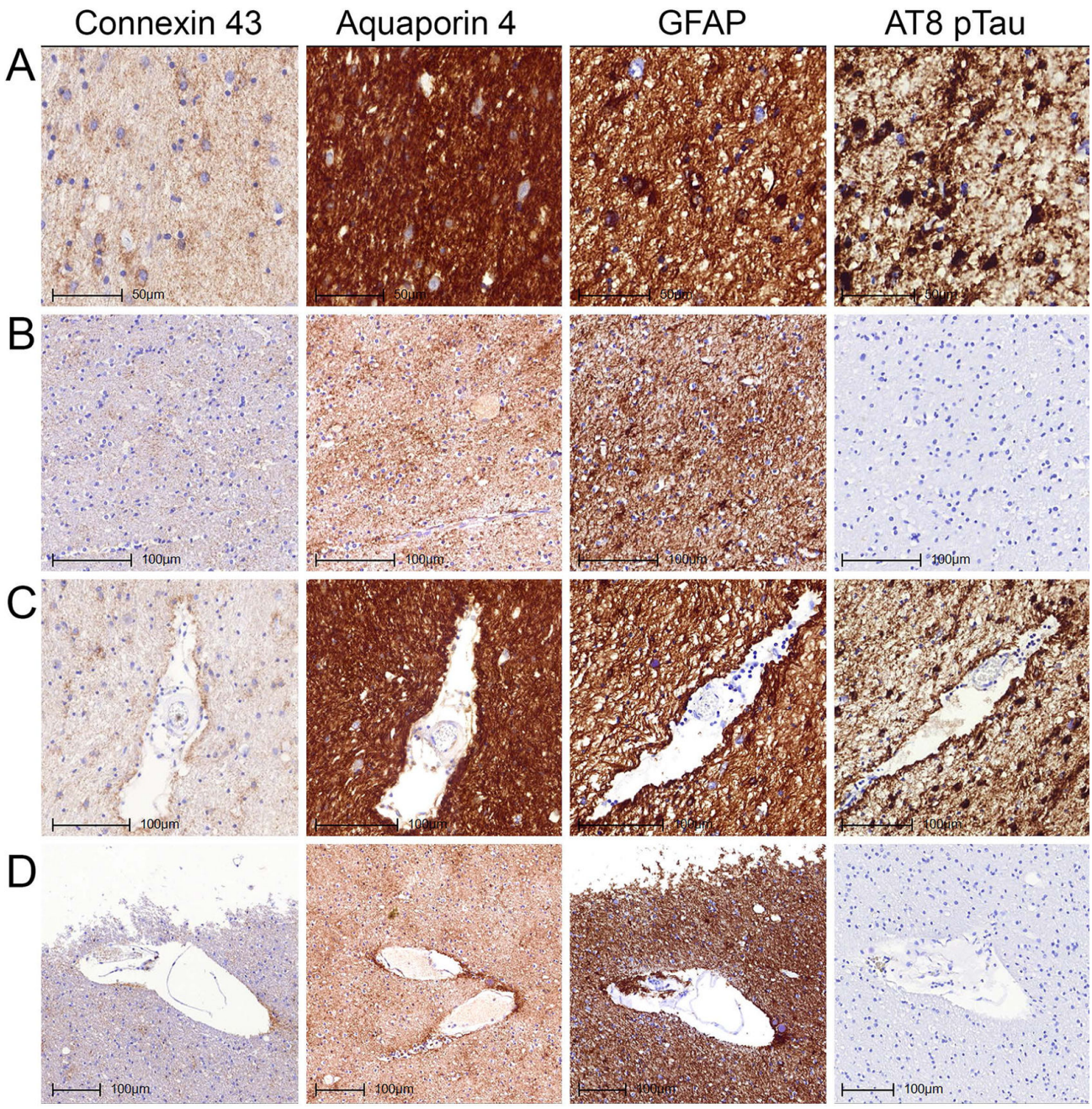

Fig 4.

Immunostaining patterns of Cx43, AQP4, GFAP and AT8 pTau in the white matter of the temporal lobe without (A, B) and with (C, D) a vessel representing different degrees of tau pathologies. Images A and C represent case ARTAG-2 demonstrating white matter and perivascular ARTAG; B and D represent case CO-8 lacking white matter and perivascular ARTAG.

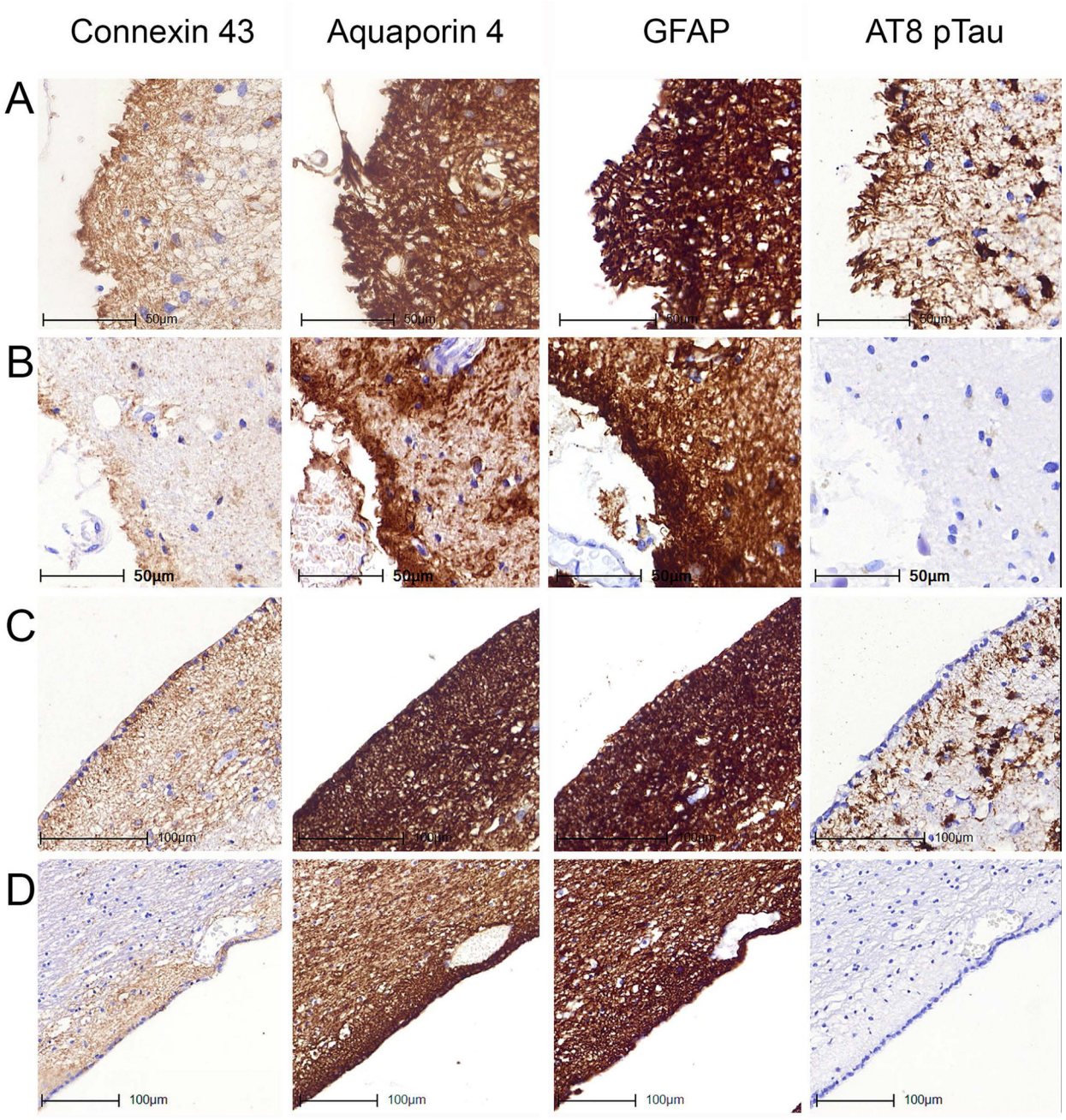

Fig 5.

Immunostaining patterns of Cx43, AQP4, GFAP and AT8 pTau in the subpial location of the inferior temporal gyrus (A, B) and the subependymal location of the inferior horn of the lateral ventricle (C, D) representing different degrees of tau pathologies. Images A and C represent case ARTAG-2 demonstrating subpial and subependymal ARTAG; B and D represent case CO-8 lacking subpial and subependymal ARTAG.

Neuropathol Appl Neurobiol. Author manuscript; available in PMC 2019 August 01.

Table 1

Demographic and neuropathological data of the cases involved in the present study.

Case Nr.	Age	Sex	Dementia	Braak stage	Thal phase	CERAD score	AGD	TDP-43
ARTAG-1	82	f	no	2	1	1	−	+
ARTAG-2	85	f	no	2	1	1	−	+
ARTAG-3	82	m	yes	5	3	2	+	+
ARTAG-4	82	f	no	3	1	1	+	+
ARTAG-5	84	f	yes	4	3	2	−	−
ARTAG-6	85	m	no	2	0	0	+	+
ARTAG-7	90	f	yes	2	0	0	−	+
ARTAG-8	87	f	yes	3	1	1	−	+
ARTAG-9	80	f	yes	3	1	1	+	+
ARTAG-10	85	f	no	2	0	0	+	+
ARTAG-11	86	f	no	3	1	1	−	+
ARTAG-12	83	f	no	3	0	0	+	+
ARTAG-13	85	m	no	1	0	0	−	−
ARTAG-14	85	m	no	2	1	1	+	−
ARTAG-15	83	f	no	3	2	1	+	−
ARTAG-16	89	m	no	3	0	0	−	−
ARTAG-17	77	m	yes	2	0	0	+	+
ARTAG-18	77	m	yes	3	2	2	+	−
ARTAG-19	87	f	yes	3	0	0	+	HS+
CO-1	86	m	no	1	0	0	−	−
CO-2	81	m	no	1	0	0	−	−
CO-3	81	f	no	3	0	0	−	−
CO-4	83	f	no	2	0	0	−	−
CO-5	79	f	no	2	0	0	−	−
CO-6	80	m	no	2	0	0	−	−
CO-7	82	m	no	2	0	0	−	−
CO-8	81	f	no	3	0	0	−	−
CO-9	84	m	no	3	0	0	−	−

Case Nr.	Age	Sex	Dementia	Braak stage	Thal phase	CERAD score	AGD	TDP-43
CO-10	81	m	no	2	0	0	–	–
CO-11	81	m	no	1	0	0	–	–
CO-12	88	f	no	2	0	0	–	–
CO-13	82	m	no	1	0	0	–	–
CO-14	83	m	no	3	0	0	–	–
CO-15	82	f	no	1	0	0	–	–
CO-16	87	m	no	1	0	0	–	–
CO-17	87	f	no	2	0	0	–	–
CO-18	83	f	no	3	0	0	–	–
CO-19	80	f	no	3	0	0	–	–
CO-20	81	m	no	3	0	0	–	–

AGD: argyrophilic grain disease; HS: hippocampal sclerosis.

Table 2

Anatomical distribution of locations examined in the present study.

		Locations				
Region	**Case**	**Subependymal**	**Subpial**	**Perivascular**	**WM**	**GM**
Hippocampus	ARTAG	9	14	9	16	21
	Control	10	9	12	11	21
Amygdala	ARTAG	5	8	10	12	13
	Control	4	10	14	14	16
Summary	ARTAG	14	22	19	28	34
	Control	14	19	26	25	37

Neuropathol Appl Neurobiol. Author manuscript; available in PMC 2019 August 01.

Neuropathol Appl Neurobiol. Author manuscript; available in PMC 2019 August 01.

Table 3

Summary of Spearman correlation tests.

		ARTAG					Control			
All locations pooled (ARTAG=117; Control=121)										
		GFAP	**Cx43**	**AT8**	**AQP4**		**GFAP**	**Cx43**	**AT8**	**AQP4**
GFAP	R	1.000	0.578	0.225	0.409	R	1.000	0.634	−0.217	0.326
	p		<0.001	0.015	<0.001	p		<0.001	0.017	<0.001
Cx43	R	0.578	1.000	0.327	0.447	R	0.634	1.000	−0.080	0.1920
	p	<0.001		<0.001	<0.001	p	<0.001		0.383	0.035
AT8	R	0.225	0.327	1.000	0.222	R	−0.217	−0.080	1.000	−0.228
	p	0.015	<0.001		0.016	p	0.017	0.383		0.012
AQP4	R	0.409	0.447	0.222	1.000	R	0.326	0.192	−0.228	1.000
	p	<0.001	<0.001	0.016		p	<0.001	0.035	0.012	
Subependymal location (ARTAG=14; Control=14)										
GFAP	R	1.000	−0.037	0.349	0.099	R	1.000	0.275	−0.191	0.323
	p		0.899	0.221	0.737	p		0.342	0.513	0.260
Cx43	R	−0.037	1.000	0.059	0.196	R	0.275	1.000	0.446	−0.200
	p	0.899		0.840	0.503	p	0.342		0.110	0.493
AT8	R	0.349	0.059	1.000	0.371	R	−0.191	0.446	1.000	−0.393
	p	0.221	0.840		0.191	p	0.513	0.110		0.164
AQP4	R	0.099	0.196	0.371	1.000	R	0.323	−0.200	−0.393	1.000
	p	0.737	0.503	0.191		p	0.260	0.493	0.164	
Subpial location (ARTAG=2; Control=19)										
GFAP	R	1.000	0.434	0.484	0.639	R	1.000	0.586	0.172	−0.168
	p		0.043	0.022	0.001	p		0.008	0.482	0.491
Cx43	R	0.434	1.000	0.403	0.525	R	0.586	1.000	−0.078	−0.207
	p	0.043		0.063	0.012	p	0.008		0.751	0.395
AT8	R	0.484	0.403	1.000	0.351	R	0.172	−0.078	1.000	−0.161
	p	0.022	0.063		0.110	p	0.482	0.751		0.509

		ARTAG				Control				
All locations pooled (ARTAG=117; Control=121)										
		GFAP	**Cx43**	**AT8**	**AQP4**		**GFAP**	**Cx43**	**AT8**	**AQP4**
AQP4	R	0.639	0.525	0.351	1.000	R	−0.168	−0.207	−0.161	1.000
	p	0.001	0.012	0.110		p	0.491	0.395	0.509	
Perivascular location (ARTAG=19; Control=26)										
GFAP	R	1.000	0.465	0.319	0.549	R	1.000	0.512	−0.132	0.143
	p		0.045	0.183	0.015	p		0.008	0.519	0.485
Cx43	R	0.465	1.000	0.600	0.795	R	0.512	1.000	0.157	0.370
	p	0.045		0.007	<0.001	p	0.008		0.444	0.063
AT8	R	0.319	0.600	1.000	0.404	R	−0.132	0.157	1.000	0.136
	p	0.183	0.007		0.087	p	0.519	0.444		0.509
AQP4	R	0.549	0.795	0.404	1.000	R	0.143	0.370	0.136	1.000
	p	0.015	<0.001	0.087		p	0.485	0.063	0.509	
White matter (ARTAG=28; Control=25)										
GFAP	R	1.000	0.742	0.659	0.625	R	1.000	0.530	0.070	0.552
	p		<0.001	<0.001	<0.001	p		0.006	0.740	0.004
Cx43	R	0.742	1.000	0.540	0.470	R	0.530	1.000	−0.075	0.026
	p	<0.001		0.003	0.012	p	0.006		0.723	0.901
AT8	R	0.659	0.540	1.000	0.494	R	0.070	−0.075	1.000	−0.203
	p	<0.001	0.003		0.008	p	0.740	0.723		0.330
AQP4	R	0.625	0.470	0.494	1.000	R	0.552	0.026	−0.203	1.000
	p	<0.001	0.012	0.008		p	0.004	0.901	0.330	
Gray matter (ARTAG=34; Control=37)										
GFAP	R	1.000	0.719	0.313	0.089	R	1.000	0.463	−0.363	0.266
	p		<0.001	0.072	0.615	p		0.004	0.027	0.112
Cx43	R	0.719	1.000	0.456	0.401	R	0.463	1.000	−0.122	0.082
	p	<0.001		0.007	0.019	p	0.004		0.471	0.629

		ARTAG				Control			
		All locations pooled (ARTAG=117; Control=121)							
		GFAP	Cx43	AT8	AQP4	GFAP	Cx43	AT8	AQP4
AT8	R	0.313	0.456	1.000	0.289	−0.363	−0.122	1.000	−0.116
	p	0.072	0.007		0.097	0.027	0.471		0.495
AQP4	R	0.089	0.401	0.289	1.000	0.266	0.082	−0.116	1.000
	p	0.615	0.019	0.097		0.112	0.629	0.495	